Molecular determinants of glycine receptor $\alpha\beta$ subunit sensitivities to Zn^{2+}-mediated inhibition

Paul S. Miller[1], Marco Beato[1], Robert J. Harvey[2] and Trevor G. Smart[1]

[1]*Department of Pharmacology, University College London, Gower Street, London WC1E 6BT, UK*

[2]*Department of Pharmacology, School of Pharmacy, 29–39 Brunswick Square, London WC1N 1AX, UK*

Glycine receptors exhibit a biphasic sensitivity profile in response to Zn^{2+}-mediated modulation, with low Zn^{2+} concentrations potentiating ($< 10\,\mu$M), and higher Zn^{2+} concentrations inhibiting submaximal responses to glycine. Here, a substantial 30-fold increase in sensitivity to Zn^{2+}-mediated inhibition was apparent for the homomeric glycine receptor (GlyR) α1 subunit compared to either GlyR α2 or α3 subtypes. Swapping the divergent histidine (H107) residue in GlyR α1, which together with the conserved H109 forms part of an intersubunit Zn^{2+}-binding site, for the equivalent asparagine residue present in GlyR α2 and α3, reversed this phenotype. Co-expression of heteromeric GlyR α1 or α2 with the ancillary β subunit yielded receptors that maintained their distinctive sensitivities to Zn^{2+} inhibition. However, GlyR α2β heteromers were consistently 2-fold more sensitive to inhibition compared to the GlyR α2 homomer. Comparative studies to elucidate the specific residue in the β subunit responsible for this differential sensitivity revealed instead threonine 133 in the α1 subunit as a new vital component for Zn^{2+}-mediated inhibition. Further studies on heteromeric receptors demonstrated that a mutated β subunit could indeed affect Zn^{2+}-mediated inhibition but only from one side of the intersubunit Zn^{2+}-binding site, equivalent to the GlyR α1 H107 face. This strongly suggests that the α subunit is responsible for Zn^{2+}-mediated inhibition and that this is effectively transduced, asymmetrically, from the side of the Zn^{2+}-binding site where H109 and T133 are located.

The glycine receptor (GlyR) is a prominent inhibitory synaptic receptor of the mammalian hindbrain and spinal cord (Aprison & Daly, 1978). This pentameric receptor consists of ligand-binding α subunits and homologous structural β subunits (Pfeiffer *et al.* 1982). To date, molecular cloning has revealed four subtypes of the α subunit (α1–4) and a single variant of the β subunit (Handford *et al.* 1996). The GlyR is a founder member of the Cys loop ion channel superfamily along with the homologous γ-aminobutyric acid type A (GABA$_A$), nicotinic acetylcholine (nACh) and serotonin type 3 (5HT3) receptors (Grenningloh *et al.* 1987).

GlyRs are targets for a number of different modulators, including ethanol and anaesthetics (Celentano *et al.* 1988; Harrison *et al.* 1993), picrotoxin (Schmieden *et al.* 1989) and Zn^{2+} (Bloomenthal *et al.* 1994). This divalent cation exerts a complex biphasic modulation of recombinant α1, α2 and α1β GlyRs and also of native GlyRs from spinal cord neurones (Bloomenthal *et al.* 1994; Laube *et al.* 1995). Modulation by Zn^{2+} potentiates GlyR activation at low concentrations (0.1–10 μM) and attenuates

sensitivity to glycine at higher concentrations ($> 10\,\mu$M). These actions could be physiologically relevant as Zn^{2+} is concentrated in selected nerve terminals and packaged into synaptic vesicles. Moreover, it may be released into the synaptic cleft or form a thin 'Zn^{2+} veneer' following nerve fibre stimulation (Assaf & Chung, 1984; Howell *et al.* 1984; Frederickson *et al.* 2000; Kay, 2003) resulting in multiple effects on neuronal excitability by modulating ion channels (Smart *et al.* 1994; Harrison & Gibbons, 1994; Smart *et al.* 2004).

An inhibitory Zn^{2+}-binding site has been proposed on GlyR α1 that involves Zn^{2+} coordination by two histidine residues, H107 and H109 (Harvey *et al.* 1999) with the potential involvement of T112 (Laube *et al.* 2000). More recently, co-expression of mixed GlyR α1 point-mutated subunits suggested that the H107 and H109 residues are contributed from adjacent α subunits (Nevin *et al.* 2003) forming an intersubunit Zn^{2+}-binding site, with T112 probably playing a less direct, general structural role. Sequence alignments of GlyR subunits reveal that the equivalent position to H107 in all other GlyR subtypes

is occupied by an asparagine residue, though previously no difference in sensitivity to Zn^{2+}-mediated inhibition has been detected between GlyR $\alpha1$ and $\alpha2$ (Laube *et al.* 1995). This contrasts with recombinant $GABA_A$ receptors, which demonstrate differential sensitivities to inhibitory Zn^{2+} determined by their subunit composition (Draguhn *et al.* 1990; Smart *et al.* 1991; Hosie *et al.* 2003).

In this study, we report a large difference in the potency of Zn^{2+}-mediated inhibition at GlyR $\alpha1$ compared to the GlyR $\alpha2$ and $\alpha3$ subtypes and additionally elucidate a novel residue, T133, in the GlyR $\alpha1$ subunit that is critical for inhibition by Zn^{2+}. Additionally, the role of the GlyR β subunit in influencing the effects of Zn^{2+}-mediated inhibition revealed a functional asymmetry to the Zn^{2+}-binding site with the GlyR $\alpha1$ H109, T133 'face' forming a vital transduction component required for the inhibitory modulation by Zn^{2+}.

Methods

cDNA constructs

Wild-type cDNA constructs that were used included the human (h) GlyR $\alpha1L$ (long, or $\alpha1^{INS}$), hGlyR $\alpha2A$ and rat (r) GlyR $\alpha3S$ (short) splice variants, and the hGlyR β subunit. Site-directed mutagenesis was performed using the Stratagene Quikchange kit. The mutated sequences were confirmed by complete sequencing of the cDNA inserts using an ABI sequencer.

Cell culture and transfection

Human embryonic kidney (HEK) cells (ATCC CRL1573) were grown in Dulbecco's modified Eagle's medium (DMEM) supplemented with 10% fetal calf serum (FCS), 2 mM glutamine, 100 units ml^{-1} penicillin G and 100 $\mu g\, ml^{-1}$ streptomycin, incubated at $37^{\circ}C$ in 95% air-5% CO_2 (Smart *et al.* 1991). HEK cells were transfected by electroporation at 400 V, infinite resistance and 125 μF, using a Biorad Gene Electropulser II. Plasmids were cotransfected in a 1 : 1 ratio with a plasmid for the reporter, enhanced green fluorescent protein (GFP). To ensure co-expression of GlyR $\alpha\beta$ heteromers, the GlyR β subunit expression construct was mixed with GlyR α subunit plasmids at a ratio of 30 : 1. Cells were plated onto poly-L-lysine-coated coverslips (100 $\mu g\, ml^{-1}$ poly-L-lysine) sufficient to achieve 20% confluence and used for electrophysiology the day after transfection.

Neuronal cell culture and acute spinal cord slice preparation

In accordance with UK leglislation, embryonic day 15 (E15) embryos were extracted from Sprague-Dawley rats by Caesarean section and placed in ice-cold phosphate-buffered saline (PBS). The spinal columns were excised and separated from the meninges and dorsal root ganglia. Spinal cords were cut into four sections and treated with 0.25% w/v trypsin in Earle's balanced salt solution (EBSS) for 15 min at $37^{\circ}C$. The tissue was then washed three times in EBSS to remove residual trypsin and sequentially triturated using fire-polished Pasteur pipettes of narrowing tip diameter. Spinal cord cell suspensions were then centrifuged at 500 g for 5 min and resuspended in DMEM plating medium supplemented per 100 ml with 5 ml FCS, 5 ml horse serum (HS), 0.6% w/v L-glucose (Sigma) and 0.04% w/v $NaHCO_3$. Cells were plated at a density of 5×10^5 per coverslip precoated either with poly-L-lysine alone, or also with an astrocyte monolayer. After 4 days the primary culture medium was replaced with Neurobasal medium (Invitrogen) supplemented with 1% v/v B-27 supplement (Invitrogen) 0.25% v/v of 200 mM L-glutamine, 1 ng ml^{-1} recombinant rat ciliary neurotrophic factor (CNTF, Peprotech, London, UK) and 100 pg ml^{-1} recombinant glial cell line-derived neurotrophic factor (GDNF; Peprotech). This medium was replenished twice weekly.

Acute spinal cord slices (350 μm thickness) were obtained from postnatal day P0–P1 or P17–P18 rats. Briefly, the animal was anaesthetized with an intraperitoneal injection of urethane (10% w/v, Sigma) and decapitated. After ventral laminectomy, the spinal cord (from mid-thoracic to lumbar region) was removed and fixed vertically to an agar block using tissue glue (Vetbond, WPI Scientific Instruments). The block was glued to the base of the slicing chamber of a Leica VT1000 vibratome and eight to ten slices were taken from the lumbar region spanning the L2–L5 segments. After 30 min of incubation at $37^{\circ}C$, the slices were allowed to cool to, and then maintained at, room temperature ($20–22^{\circ}C$) for another 30 min. Individual slices were then transferred to the recording chamber and superfused with Krebs solution continuously gassed with 95% O_2–5% CO_2.

Solutions

For the cultured cells, the internal patch pipette solution contained (mM): KCl 140, $MgCl_2$ 2, $CaCl_2$ 1, Hepes 10, EGTA 11 and ATP 2; pH 7.11 for HEK cells and pH 7.3 (with NaOH) for spinal cord primary cultures ($\sim$300 mosmol l^{-1}). The Krebs solution consisted of (mM): NaCl 140, KCl 4.7, $MgCl_2$ 1.2, $CaCl_2$ 2.5, Hepes 10 and D-glucose 11; pH 7.4 ($\sim$ 300 mosmol l^{-1}). Primary cultured neuronal cells were superfused in Krebs solution containing: 0.5 μM tetrodotoxin (TTX), 10 μM bicuculline, 20 μM 2-amino-5-phosphovalerate (AP5) and 10 μM 6-cyano-2,3-nitroquinoxalinedione (CNQX) to abolish action potentials and synaptic $GABA_A$ and glutamate receptor activation.

The dissection and Krebs solutions used for the acute spinal cord slices were identical and composed of (mM): NaCl 113, KCl 3, NaHCO$_3$ 25, NaH$_2$PO$_4$ 1, CaCl$_2$ 2, MgCl$_2$ 2 and D-glucose 11. The patch pipette solution used for the slices contained (mM): CsCl 140, NaCl 4, MgCl$_2$ 1, CaCl$_2$ 0.5, EGTA 5, Hepes 10 and Mg-ATP 2; pH adjusted to 7.3 using CsOH.

Electrophysiology

An Axopatch 200B amplifier (Axon Instruments) was used to record whole-cell currents from single HEK cells or spinal cord primary cultures using the patch-clamp technique. HEK cells exhibited resting potentials between -10 and -40 mV and were voltage clamped at -40 mV. Healthy spinal cord neurones were judged on the basis of robust dendritic networking, resting potentials of -50 to -70 mV and steady holding currents of < 10 pA. These cells were clamped at -70 mV and series resistance compensation of 70–90% was employed. All cells were visualized with a differential interference contrast Nikon microscope and an epifluorescence attachment was used to identify GFP-transfected HEK cells. A Y-tube was used to rapidly apply drugs and Krebs solution (exchange rate approximately 50–100 ms) to patch-clamped cells. Patch electrodes were fabricated using a Narashige PC-10 puller with resistances after polishing of 4–5 MΩ. All recordings were performed in constantly perfusing Krebs solution at room temperature.

Recordings from acute spinal cord slices were performed from motoneurones visually identified with infra-red differential interference contrast microscopy on the basis of their ventral location and morphology. Electrodes were pulled with 1–1.5 MΩ resistance and fire polished to a final resistance of approximately 2.5 MΩ. Cells were voltage clamped at -70 mV and only those cells with stable holding currents (< 40 pA) for the duration of the experiment were included for analysis. Series resistance (6–10 MΩ) was routinely compensated (70–90%). Glycine (30 μM, with or without Zn²⁺) was applied via a Y-tube at intervals of 2 min for the duration of the experiment before, during and after pre-incubation with 30 μM Zn²⁺. Cells were included in the analysis only if the response to glycine recovered after application of Zn²⁺, to within 90–110% of the control response. The Krebs solution contained 0.5 μM TTX, 5 μM SR95531 hydrobromide (GABA$_A$ receptor antagonist), 20 μM AP5 and 10 μM CNQX to pharmacologically isolate glycine currents.

Data acquisition and analysis

All currents were filtered at 3 kHz using a Bessel filter (-36 dB per octave). Data were recorded in 20 s acquisition episodes directly to a Pentium IV, 1.8 GHz computer into Clampex 8.0 via a Digidata 1322A (Axon Instruments) sampling at 200 μs intervals. Ligand-induced responses were assessed by sequentially applying a concentration of the test drug, twice, between control responses evoked by EC$_{50}$ values of the agonist to assess the response stability during the experiments. For the pre-application experiments, Zn²⁺ was applied for 15 s prior to glycine application and then followed by a 2 min recovery in Krebs solution prior to further drug applications. If the control responses varied by less than 15% from each other, then the test responses were normalized by linear interpolation between the two surrounding control responses. Digitized current records were analysed off-line using Axoscope 8.2. Biphasic Zn²⁺ concentration–response curves were fitted as previously described (Miller et al. 2004) and the glycine concentration–response curves were fitted with the Hill equation:

$$I/I_{max} = \left[\left(1/1 + (EC_{50}/A)^n\right)\right],$$

where EC$_{50}$ represents the concentration of glycine (A) inducing 50% of the maximal current evoked by a saturating concentration of glycine and n is the Hill coefficient. The glycine concentration–response data were normalized to the maximum response to glycine. The Zn²⁺ dose–response data were normalized to the control glycine response amplitude in the absence of Zn²⁺. The competitive-type inhibition caused by Zn²⁺ was analysed according to the method of Arunlakshana & Schild (1959). Full glycine concentration–response curves were obtained in each HEK cell and then at least one and usually more curves were obtained in the presence of 50, 100, 200 and 500 μM Zn²⁺. The curves were tested for parallelity and the dose ratios (DRs) for glycine were calculated from the respective glycine EC$_{50}$ values. The mean dose ratios for each Zn²⁺ concentration (B) allowed the dissociation constant for Zn²⁺ (K_B) to be determined using the transformed Schild equation:

$$\log(DR - 1) = \log B - \log K_B,$$

The slope of the Schild plot of log (DR − 1) *versus* log(B) was not significantly different from unity ($P < 0.05$). The slope was then constrained to unity and the intercept on the abscissa used to determine the pA_2 ($= -\log K_B$) for Zn²⁺. All statistical comparisons used an unpaired t test.

Modelling

The mature N-terminal extracellular domain (ECD) of the human GlyR α2 subunit, was modelled on the crystal structure of the acetylcholine binding protein (AChBP; Brejc et al. 2001) using SwissProt DeepView in accordance with a ClustalW protein alignment.

Results

Differential Zn²⁺ sensitivity between GlyR α1 and GlyR α2 subunits

A comparison of the sensitivities of GlyRs to Zn^{2+}-mediated inhibition was initiated because one of the key Zn^{2+}-binding residues we reported previously, H107, is present in the GlyR α1 but not in the GlyR α2 subtype (Harvey *et al.* 1999). Modulation by Zn^{2+} was examined using two different protocols. The first involved co-application of varying concentrations of Zn^{2+} with a concentration of glycine equivalent to the EC_{50}. The degree of inhibition was measured for the peak glycine response (I_{peak}) and then 4 s after the co-application (I_4) to reveal a delayed onset of inhibition (Fig. 1A–C). The second protocol utilized the pre-incubation of Zn^{2+} and only the peak responses to glycine were measured as pre-incubation allowed Zn^{2+} to equilibrate with the GlyR (Fig. 1D). Irrespective of the protocol, all Zn^{2+} concentration–response curves exhibited a biphasic shape due to the potentiating and inhibitory effects of Zn^{2+} on GlyRs. Using these procedures, a clear difference in

the potency of inhibitory Zn^{2+} was observed between GlyR α1 and GlyR α2 subunits. Under pre-incubation conditions both receptors could be inhibited but there was a 25-fold reduction in Zn^{2+} potency for GlyR α2 (IC_{50}, $360 \pm 40\,\mu M$; $n = 11$) compared to GlyR α1 (IC_{50}, $15 \pm 2\,\mu M$; $n = 5$; $P < 0.05$; Table 1). All subsequent experiments utilized the pre-incubation protocol with Zn^{2+}.

Histidine 107 is responsible for differential Zn²⁺ sensitivity between GlyR α subunits

Comparing the N-terminal extracellular domains of the GlyRs reveals that GlyR α2, like all other α variants except GlyR α1, retains an asparagine (N114) residue at the homologous position to the putative Zn^{2+}-binding residue, H107, in the GlyR α1 subunit (Fig. 2A). If H107 coordinates Zn^{2+}, then the divergent N114 in GlyR α2 could be responsible for the differential sensitivity to Zn^{2+} as asparagines are poor coordinators for this cation (Auld, 2001). This was examined by exchanging residues between the GlyR α1 and α2 subunits at the equivalent positions
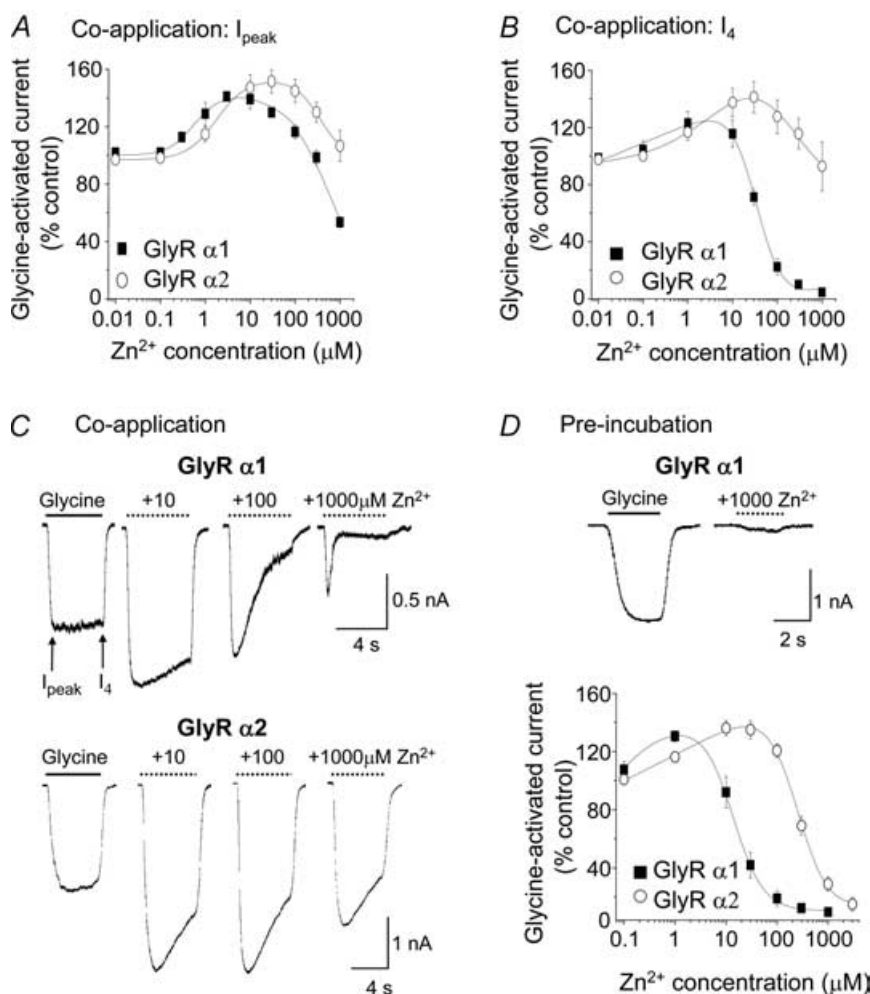

Figure 1. Differential inhibition of glycine-activated currents by Zn²⁺ at GlyR α1 and GlyR α2
A, Zn^{2+} concentration–response curves for the modulation of peak (I_{peak}) glycine-evoked currents (EC_{50}: GlyR α1, $20\,\mu M$; GlyR α2, $70\,\mu M$) following a 4 s co-application of glycine and Zn^{2+}. *B*, Zn^{2+} concentration–response curves as in *A* with the current amplitudes measured at the end of the co-application (I_4). *C*, membrane currents comparing glycine-activated I_{peak} and I_4 for GlyR α1 (upper traces) and GlyR α2 (lower traces) after applying glycine (EC_{50}) in the absence and presence of co-applied 10, 100 and 1000 μM Zn^{2+}. *D*, glycine-activated I_{peak} following co-application of glycine (EC_{50}) and Zn^{2+} after prior incubation for 15 s with an equivalent concentration of Zn^{2+} for GlyR α1 and GlyR α2. The inset shows typical glycine-activated currents for GlyR α1 in the absence and presence of 1000 μM Zn^{2+} under the pre-incubation protocol. $n = 6$–13 for all experiments. All points in this and succeeding figures represent the mean ± S.E.M.

Table 1. GlyR sensitivities to glycine and Zn^{2+}

GlyR subtype	Gly EC$_{50}$ (μM)	I_{max} (nA)	n	Zn^{2+} IC$_{50}$ (μM)	n
α1	24 $\pm$ 5	4.5 $\pm$ 0.5	10	15 $\pm$ 2	5
α2	66 $\pm$ 6	3.7 $\pm$ 0.5	13	360 $\pm$ 40	11
α1 β	18 $\pm$3	4.5 $\pm$ 0.9	6	13 $\pm$ 2	3
α2 β	51 $\pm$ 4	5.6 $\pm$ 0.5	3	180 $\pm$ 30	13
α1^{H107N}	24 $\pm$ 2	5.9 $\pm$ 0.3	4	230 $\pm$ 30	5
α1^{H109F}	56 $\pm$ 5	5.1 $\pm$ 0.2	3	> 1 mM	3
α1^{T133A}	130 $\pm$ 30	4.8 $\pm$ 0.7	5	> 1 mM	5
α1^{T135A}	17 $\pm$ 2	3.3 $\pm$ 0.6	3	26 $\pm$ 6	3
α1^{H107N} β^{N130H}	28 $\pm$ 8	4.8 $\pm$ 0.8	3	24 $\pm$ 3	5
α1^{H109F} β^{S156T}	39 $\pm$ 4	5.2 $\pm$ 1.2	3	> 1 mM	3
α1^{T133A} β^{S156T}	90 $\pm$ 16	3.2 $\pm$ 0.9	3	> 1 mM	3
α1 β^{S156A}	44 $\pm$ 9	5.9 $\pm$ 0.7	3	17 $\pm$ 7	3
α2^{N114H}	58 $\pm$ 3	4.2 $\pm$ 0.7	3	29 $\pm$ 2	4
α2 β^{G128S}	52 $\pm$ 5	5.0 $\pm$ 1.6	3	170 $\pm$ 20	4
α2 β^{S156T}	47 $\pm$ 9	5.6 $\pm$ 1.4	3	210 $\pm$ 20	5
α3	48 $\pm$ 3	5.3 $\pm$ 1.3	4	150 $\pm$ 10	4
α3^{N107H}	53 $\pm$ 12	5.3 $\pm$ 0.8	5	26 $\pm$ 7	3
sc 5 DIV	$\sim$ 40	3.1 $\pm$ 0.3	12	320 $\pm$ 50	8
sc 7 DIV	$\sim$ 30	4.9 $\pm$ 0.7	12	110 $\pm$ 10	8
sc 10–14 DIV	$\sim$ 30	4.3 $\pm$ 0.4	8	88 $\pm$ 21	8

The values indicate the glycine EC$_{50}$ values for activating the recombinant and native GlyRs and also the Zn^{2+} IC$_{50}$ values for modulating the half-maximal glycine-activated responses where Zn^{2+} is first pre-equilibrated with the receptor for 15 s before an equivalent concentration of Zn^{2+} is coapplied with glycine. All numbers are means $\pm$ S.E.M. from n cells. For the native GlyR in spinal cord (sc) neurones, the EC$_{50}$ values were estimated from linear segments of the dose–response curves.

of H107 (α1) and N114 (α2) to generate α1^{H107N} and α2^{N114H}. This exchange reversed the sensitivities of the GlyR α1 and α2 subunits with regard to Zn^{2+} inhibition, such that α1^{H107N} (IC$_{50}$, 230 $\pm$ 40 μM; $n = 5$) was now 8-fold less sensitive to Zn^{2+} compared to α2^{N114H} (IC$_{50}$, 29 $\pm$ 2 μM; $n = 4$; Fig. 2B; Table 1). Taken together this strongly suggests that H107 not only forms part of the inhibitory Zn^{2+}-binding site but also is largely responsible for the different sensitivities of the GlyR α1 and GlyR α2 subunits to Zn^{2+} inhibition.

To further establish the significance of H107 in the subtype sensitivity to Zn^{2+} inhibition, GlyR α3 subunits, which possess an asparagine residue at the homologous position (N107 in α3), were also examined. This is of particular relevance as currently there are no selective pharmacological blockers to distinguish between the two adult GlyR subtypes, α1 and α3. Consistent with the data for GlyR α2, the potency of Zn^{2+} was also substantially reduced on GlyR α3 (IC$_{50}$, 150 $\pm$ 10 μM; $n = 4$). In accord with the results for GlyR α2 subunits, replacing N107 with histidine in GlyR α3 subunits (α3^{N107H}) substantially increased the potency of Zn^{2+} mediated inhibition (IC$_{50}$, 26 $\pm$ 7; $n = 3$; $P < 0.05$; Fig. 2C).

Mechanism for Zn^{2+}-mediated inhibition on GlyR α1 and GlyR α2 subtypes

The proposed mechanism of Zn^{2+}-mediated inhibition has not been fully investigated, although glycine concentration–response curves determined in the presence of a single concentration of Zn^{2+} exhibit the same maximum response (Laube *et al.* 1995; Han & Wu, 1999). The mode of Zn^{2+}-mediated inhibition was characterized for both GlyR α1 and GlyR α2 subtypes by generating glycine concentration–response curves in the presence of several inhibitory concentrations of

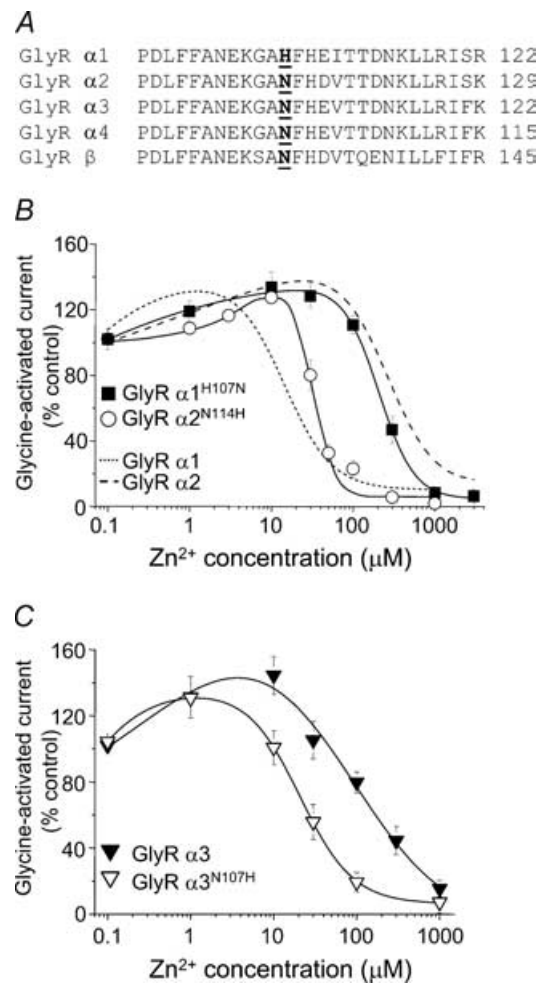**Figure 2. Reversal of GlyR α subunit sensitivities to Zn^{2+}-mediated inhibition**

A, primary amino acid sequence alignment for a segment of the N-terminal domains highlighting the unique nature of H107 in the GlyR α1 subtype. *B* and *C*, Zn^{2+} concentration–response curves for the modulation of glycine (EC$_{50}$)-activated currents for GlyR α1^{H107N} and GlyR α2^{N114H} (*B*), and GlyR α3 and GlyR α3^{N107H} (*C*) wild-type and mutant subunits. Peak glycine (EC$_{50}$)-evoked responses were measured in the absence and presence of varying concentrations of Zn^{2+} after 15 s pre-incubation with an equivalent Zn^{2+} concentration. The Zn^{2+} curves for wild-type GlyR α1 and GlyR α2 are included for comparison in (*B*) (taken from Fig. 1*D*). $n = 3$–5 for all experiments.

Zn^{2+} (Fig. 3*A* and *B*). For both GlyR α1 and GlyR α2, these curves were displaced by Zn^{2+} in a parallel manner without any significant reduction in the maximal current evoked by saturating concentrations of glycine, which is in accord with a competitive-type mechanism. In addition, due to the relatively high sensitivity of GlyR α1 to Zn^{2+}-mediated inhibition it was possible to pre-incubate
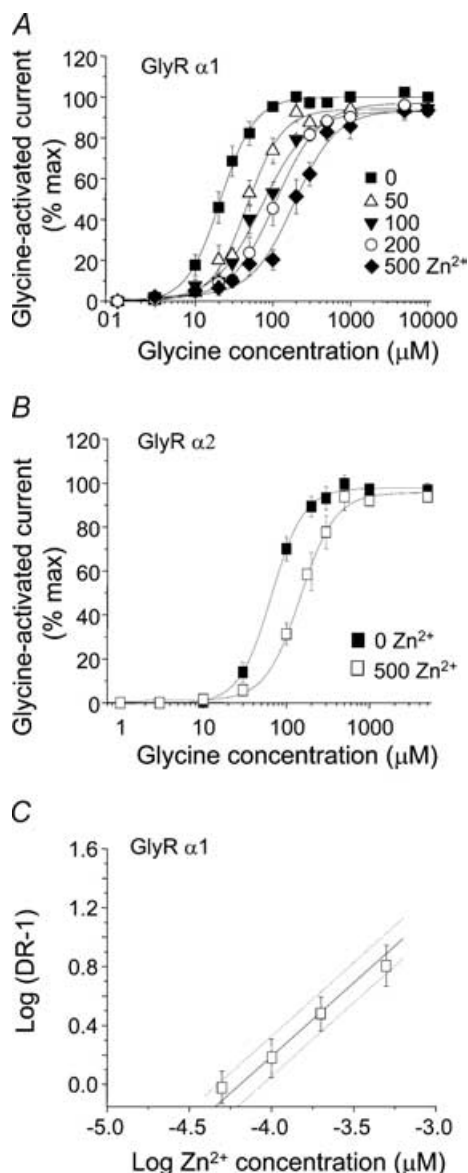

Figure 3. Zn^{2+} is a competitive inhibitor at GlyR α1 and GlyR α2
Glycine concentration–response curves for both GlyR α1 (*A*) and GlyR α2 (*B*) are displaced in a competitive-type inhibitory manner by Zn^{2+}. In all cases Zn^{2+} was co-applied with glycine (EC_{50}) after a 15 s pre-incubation with Zn^{2+}. Glycine curves for GlyR α1 were determined in the absence and presence of 50, 100, 200 and 500 μM Zn^{2+} and for GlyR α2, in the absence and presence of 500 μM Zn^{2+}. *C*, Schild analysis generated from the GlyR α1 dose ratios taken from the curves in (*A*). The continuous line indicates the constrained unity slope with 95% confidence intervals assigned by dotted lines. All experiments were from 6 to 13 cells.

at several different inhibitory Zn^{2+} concentrations and achieve measurable separation between each of the glycine concentration–response curves. This was not possible for the less sensitive GlyR α2 subunit without incurring Zn^{2+} solubility problems. A Schild analysis was then used to determine a pA_2 value for Zn^{2+} as an antagonist at the GlyR α1 subtype (Fig. 3*C*). The Schild plot slope was not significantly different from one, and the constrained slope provided a pA_2 of 4.44 ± 0.14, yielding a dissociation constant for Zn^{2+} from the inhibitory site of $27.5 \pm 0.87\ \mu$M ($n = 7$).

Rate of onset for Zn^{2+}-mediated inhibition at GlyR α1 and GlyR α2

The mechanism of action for Zn^{2+}-mediated inhibition was further investigated by analysing the rate of onset for the block by Zn^{2+} at GlyR α1 and GlyR α2. Using a pre-incubation protocol, 1000 μM Zn^{2+} caused substantial inhibition at both GlyR α1 ($90 \pm 2.4\%$; $n = 6$) and GlyR α2 ($78 \pm 4.4\%$; $n = 11$; Fig. 1*D*). During co-application, however, the level of inhibition induced by 1000 μM Zn^{2+} was dramatically different between the two GlyRs (compare current records in Fig. 1*C*). To assess the rates of onset for Zn^{2+}-mediated inhibition at GlyR α1 and α2, potency matched concentrations of Zn^{2+} (40 and 1000 μM, respectively, corresponding to approximately 70% inhibition under pre-incubation conditions) were co-applied with half-maximally effective concentrations of glycine for a 60 s period to allow Zn^{2+}-mediated inhibition to reach a steady state. A 60 s application of glycine alone revealed a biphasic desensitization profile for both GlyR α1 and α2, with initial fast desensitization time constants of 4.1 ± 0.2 s and 5.6 ± 1.3 s ($n = 6$), and slow time constants of 45.7 ± 8 s and 49.5 ± 8 s ($n = 6$), respectively (Fig. 4*A* and *C*). During the initial activation phase for glycine currents in the presence of Zn^{2+}, an enhancement was observed for both GlyR α1 and α2 due to the rapid onset of Zn^{2+}-dependent potentiation. In the case of the slowly activating GlyR α2 subtype (Mangin *et al.* 2003), the initial Zn^{2+}-mediated enhancement caused a significant decrease in the 10–90% rise time to reach steady state from 1.4 ± 0.4 s in control, to 0.5 ± 0.1 s in the presence of Zn^{2+} ($n = 5$; $P < 0.05$; Fig. 4*A* and *B*). In contrast, the control activation rate for GlyR α1 is faster than that for GlyR α2, but this rate was not increased further by Zn^{2+} (340 ± 70 ms in control and 260 ± 30 ms in Zn^{2+}; $n = 6$; $P > 0.05$; Fig. 4*A* and *B*).

Examination of the subsequent Zn^{2+}-mediated inhibition revealed that the rate of onset was indistinguishable between the two receptor subtypes. In both cases, the slow desensitization phase was completely ablated leaving only a fast decaying component. This fast phase was accelerated by 1.5- to 2-fold compared to the

previously identified fast desensitization phase in the absence of Zn^{2+}. The decay time constants changed from 4.1 ± 0.2 s to 2.8 ± 0.4 s for GlyR $\alpha1$ and from 5.6 ± 1.3 s to 3.1 ± 0.3 s for GlyR $\alpha2$ ($n = 6$; Fig. 4A and C). The final levels of inhibition achieved after 60 s in 40 and 1000 μM Zn^{2+} were not significantly different for either receptor subtype, with $63 \pm 7\%$ inhibition achieved for GlyR $\alpha1$ and $57 \pm 13\%$ for GlyR $\alpha2$ ($n = 6$), indicating that the potencies for inhibition by Zn^{2+} were indeed accurately matched. The data therefore suggest that the substitution of GlyR $\alpha1$ H107 with GlyR $\alpha2$ N114 does not interfere with the rate at which Zn^{2+} can access the inhibitory site and cause inhibition.

Differential sensitivity to Zn^{2+}-mediated inhibition is unaffected by the GlyR β subunit

The 30-fold increased sensitivity of GlyR $\alpha1$ over GlyR $\alpha2$ to Zn^{2+}-mediated inhibition makes this ion a potentially useful pharmacological tool. Whether this differential sensitivity is maintained at native neuronal GlyRs was assessed using recombinant GlyR $\alpha\beta$ heteromers, which are a major physiological subtype (Pfeiffer *et al.* 1982).

Successful co-assembly of GlyR α and β subunits was established by measuring a reduction in the sensitivity to the antagonist picrotoxin (by approximately 20-fold) compared to homomeric GlyR α subunits, as previously reported (data not shown; Pribilla *et al.* 1992; Handford *et al.* 1996). The GlyR $\alpha2\beta$ heteromers exhibited a subtle though consistent 2-fold increased sensitivity to Zn^{2+}-mediated inhibition (IC_{50}, 180 ± 30 μM; $n = 13$) compared to the GlyR $\alpha2$ homomers (360 ± 40 μM; $n = 11$; $P < 0.05$; Table 1). Consistent with the previous findings using the GlyR homomers, the GlyR $\alpha2\beta$ sensitivity to Zn^{2+} remained substantially lower when compared with GlyR $\alpha1\beta$, which retained a comparable sensitivity to the GlyR $\alpha1$ homomer (Fig. 5A, Table 1).

Spinal cord GlyRs increase their sensitivity to Zn^{2+}-mediated inhibition during development

To evaluate whether a differential sensitivity to Zn^{2+}-mediated inhibition was apparent in a native environment, the Zn^{2+} sensitivity profiles of neuronal GlyRs were assessed in embryonic spinal cord cultures and in neonatal and juvenile rat acute spinal cord slices. During
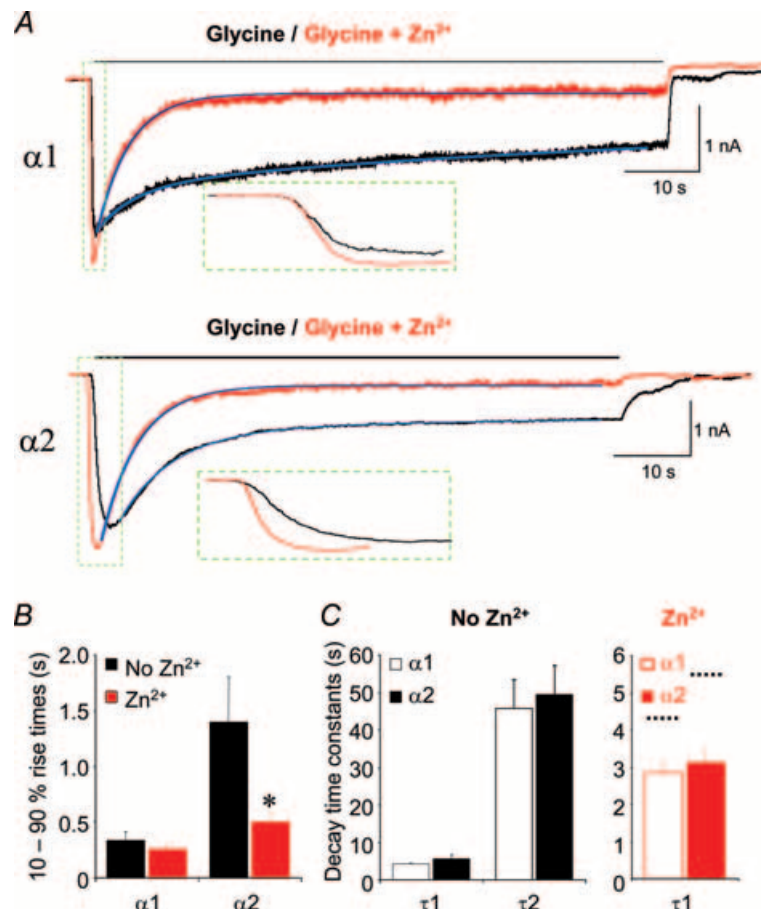

Figure 4. The effect of co-applied Zn^{2+} on the rise and decay times for glycine-activated currents on GlyR $\alpha1$ and $\alpha2$
A, glycine-activated currents during a prolonged 60 s application of half-maximally effective concentrations of glycine in the absence (black) and presence (red) of potency-matched doses of Zn^{2+} (40 and 1000 μM for GlyR $\alpha1$ and GlyR $\alpha2$, respectively). The blue lines indicate curve fits to determine the current decay times. B, 10–90% rise times in the absence and presence of the same Zn^{2+} concentrations, determined for glycine currents over the period highlighted and enlarged in the dashed green boxes in A. Note that the time for the slower activating macroscopic current of GlyR $\alpha2$ to reach steady state is markedly reduced, whilst the time for $\alpha1$ is unaffected, by Zn^{2+}. C, bar graphs revealing that GlyR $\alpha1$ and GlyR $\alpha2$ have comparable desensitization time constants. In the absence of Zn^{2+} (black bars), glycine currents decay with two time constants, fast ($\tau1$, 4–5 s) and slow ($\tau2$, 40–50 s). In the presence of Zn^{2+} (red bars), glycine currents decay with only a fast time constant (approximately 3 s), dotted black lines denote the speed of the original fast decay time constants in the absence of Zn^{2+}. $n = 3$–6. *$P < 0.05$ between the rise times for Gly $\alpha2$.

early embryonic development and in dissociated culture, the GlyR $\alpha2$ subunit appears to be the predominant α subtype, with a limited up-regulation of GlyR $\alpha1$ during the course of culture maturation (Hoch *et al.* 1989, 1992). Increased expression of the $\alpha1$ subunit becomes more evident *in vivo* during late embryonic to early postnatal developmental stages (Becker *et al.* 1988; Takahashi *et al.* 1992; Watanabe & Akagi, 1995).

Whole-cell recordings from 90% of rat spinal cord cultured neurones responded to exogenously applied glycine and multipolar neurones at 7 days *in vitro* (DIV) or older, displayed robust synaptic activity (data not shown). Neurones at 5, 7 and 10–14 DIV, all showed an overall low sensitivity to Zn^{2+}. The 5 DIV neuronal cultures especially exhibited a pharmacological profile consistent with the low Zn^{2+} sensitivity associated with the GlyR $\alpha2$ subtype (Fig. 5*B*; Table 1). To follow the period during which GlyR expression changes, electrophysiological recordings were made from neurones in acute spinal cord slices at P0–1 and P17–18. Whole-cell recordings using pre-incubation with 30 μM Zn^{2+} exhibited only a partial inhibition of the response to 30 μM glycine at P0–1 ($36 \pm 4\%$; $n = 19$). This is consistent with the presence of a mixed population

of GlyR $\alpha1$ and GlyR $\alpha2$. However, a profound inhibition ($69 \pm 4\%$; $n = 13$; Fig. 5*C* and *D*) was exhibited at P17–18, in accord with a progressive developmental transition to the adult, high Zn^{2+} sensitivity, GlyR $\alpha1$ subtype (Fig. 5*C* and *D*).

Identification of the structural elements required for Zn^{2+} inhibition

Inspecting the aligned primary sequences for GlyR α and β subunits reveals that the GlyR β subunit, like the $\alpha2$ subunit, also retains the low affinity asparagine residue at the homologous position to the Zn^{2+}-binding GlyR $\alpha1$ subunit H107 (Fig. 2*A*). This was of interest as co-expression of the β subunit with the GlyR $\alpha2$ subunit in this study caused a modest increase in sensitivity to Zn^{2+} inhibition, suggesting that the β subunit may actually contribute to the Zn^{2+}-binding site. Such a β subunit-dependent increase in sensitivity was not observed for the $\alpha1\beta$ heteromer, possibly because the $\alpha1$ subunit already possesses a higher sensitivity to Zn^{2+} realized through the presence of its unique residue, H107.
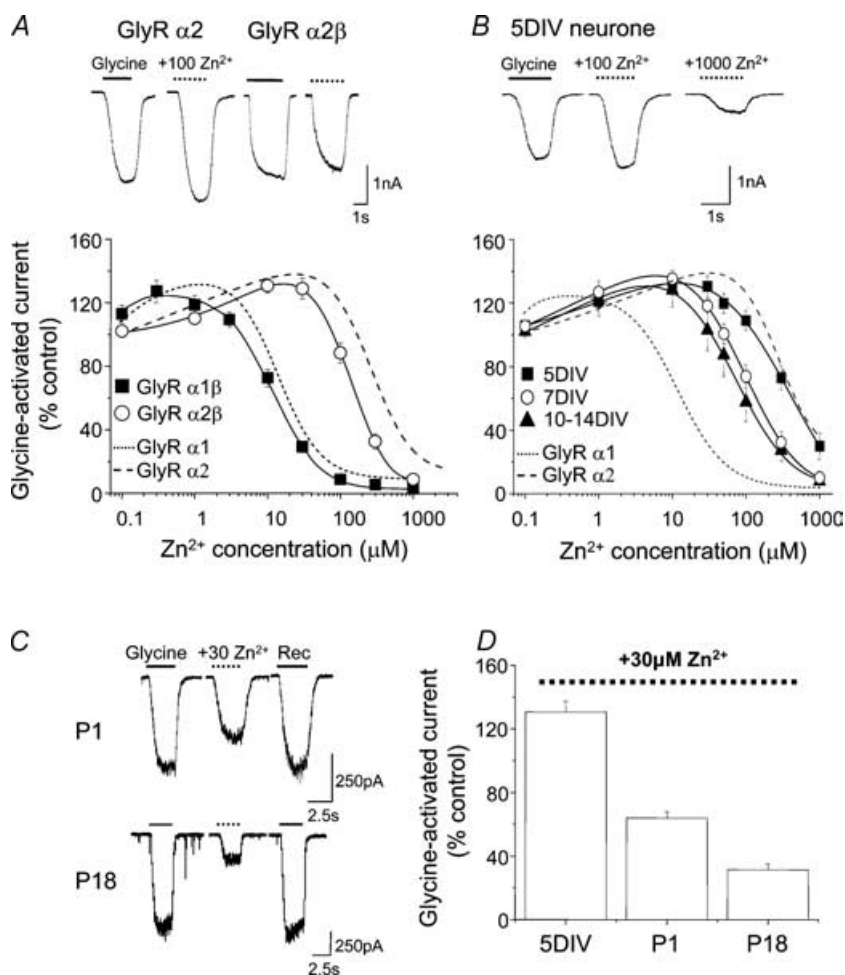

Figure 5. Differential sensitivity to inhibitory Zn^{2+} in recombinant heteromeric GlyRs and neuronal GlyRs
A, Zn^{2+} concentration–response curves for the modulation of glycine (EC$_{50}$) responses on GlyR $\alpha1\beta$ and GlyR $\alpha2\beta$ heteromers in the presence of varying concentrations of Zn^{2+} after initial Zn^{2+} pre-incubation. For comparison, the Zn^{2+} sensitivities of GlyR $\alpha1$ and GlyR $\alpha2$ homomers are shown (taken from the curve fits in Fig. 1*D*). The inset shows typical currents activated by EC$_{50}$ values of glycine on GlyR $\alpha2$ and GlyR $\alpha2\beta$, respectively, in the absence and presence of 100 μM Zn^{2+}. *B*, Zn^{2+} concentration–response curves for native GlyRs determined on rat spinal cord cultures at 5, 7 and 10–14 DIV. The inset currents illustrate the lower sensitivity of glycine (EC$_{50}$) responses to Zn^{2+}-mediated inhibition in a 5 DIV spinal cord neurone. *C*, glycine-activated currents in the absence and presence of 30 μM Zn^{2+} and following recovery after 10 min for a neonatal (P1) and juvenile (P18) neurone. *D*, bar graph illustrating the effect of 30 μM pre-applied Zn^{2+} on glycine (EC$_{50}$)-activated currents recorded from neurones at 5 DIV in culture and in spinal cord slices at P1 and P18. In all experiments $n = 3$–19.

A directed comparative scan was therefore made of the $\alpha2$ and β subunit primary amino acid sequences guided by modelling the GlyR N-terminal domains on the crystal structure of the homologous acetylcholine binding protein (AChBP; Brejc *et al.* 2001). This approach identified key differences in amino acids in the predicted vicinity of the GlyR $\alpha1$ H107- and H109-based Zn^{2+} inhibitory binding site. Of these, only two residues differed that might impact on Zn^{2+} coordination at this site. In GlyR $\alpha2$ subunits, G112 ($\alpha1$ G105) and T140 ($\alpha1$ T133) are replaced in the β subunit by S128 and S156, respectively (Fig. 6*A* and *B*). In view of their proximity to the Zn^{2+} inhibitory site and to elucidate the cause of the β subunit-induced increase in GlyR $\alpha2$ sensitivity to Zn^{2+} inhibition, the β subunit residues were switched for their $\alpha2$ subunit counterparts forming the mutants, GlyR β^{S128G} and β^{S156T}. However, neither GlyR β^{S128G} nor β^{S156T} affected the ability of the β subunit to increase GlyR $\alpha2$ sensitivity to Zn^{2+} (Fig. 6*C* and Table 1).

Using the homology model for the GlyR, no other suitable β subunit residues capable of interacting with the Zn^{2+} inhibitory site were identified. The effect of the β subunit on GlyR $\alpha2$ was presumed to reflect an indirect structural effect akin to the role suggested for T112 in the GlyR $\alpha1$ subunit (Nevin *et al.* 2003), which also affected the sensitivity to Zn^{2+}-mediated inhibition (Laube *et al.* 2000). However, by conducting similar structural comparisons for the GlyR $\alpha1$ subunits revealed that a T133 residue, located on β strand 6 (according to the nomenclature of Brejc *et al.* 2001), was predicted to reside directly below H109 on β strand 5. Moreover, another threonine in GlyR $\alpha1$, T135, is also located on
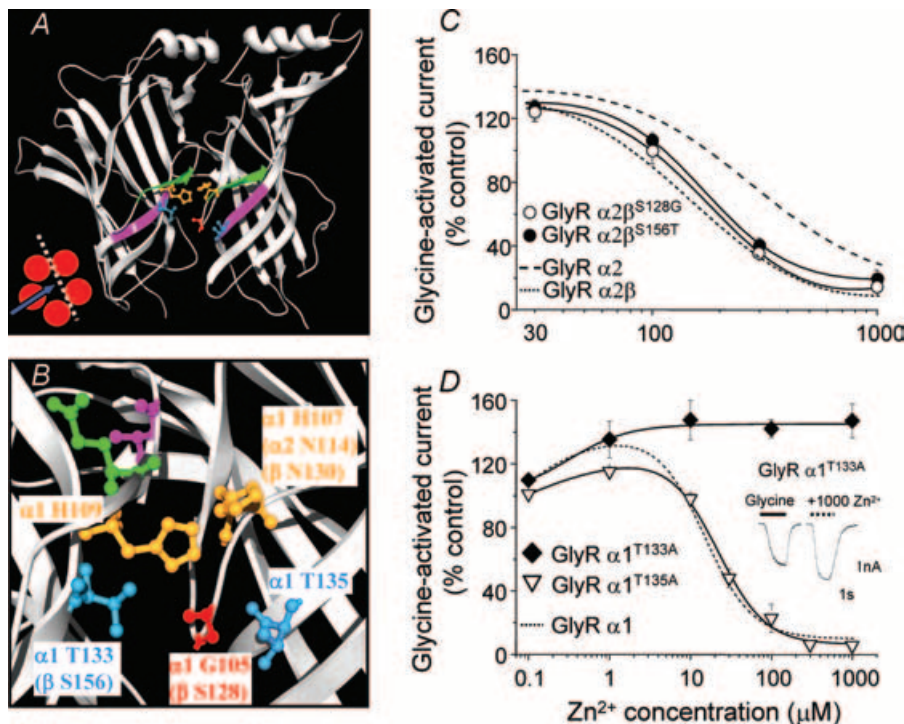

Figure 6. Evaluation of potential binding residues in the immediate vicinity of the inhibitory Zn^{2+} site
A, two neighbouring GlyR $\alpha1$ subunits modelled on the AChBP and viewed from the inside face (see inset); expanded in *B*, to highlight inhibitory Zn^{2+}-binding site residues, H107 and H109 (orange) and two newly identified potential Zn^{2+}-binding residues, T133 and T135 (blue). An additional variant residue in the β subunit, S128, is also shown (red). The β-strand 5 (green) containing H107 and H109 is presented directly above β-strand 6 (pink) containing T133 and T135. *B*, homologous residues are shown in parentheses. For reference, GlyR $\alpha1$ E110 (green) and T112 (pink), previously shown (Laube *et al.* 2000) to influence Zn^{2+}-mediated inhibition, are included and are both predicted to face away from the site, suggesting the side chains of these residues are unlikely to directly coordinate Zn^{2+}. *C*, assessment of β subunit residues that may be responsible for the increased sensitivity to Zn^{2+}-mediated inhibition on the GlyR $\alpha2$ subtype by measuring Zn^{2+} modulation of half-maximally effective glycine responses (using the pre-incubation protocol) on GlyR $\alpha2\beta^{S128G}$ and GlyR $\alpha2\beta^{S156T}$ heteromers. The curves for GlyR $\alpha2$ and GlyR $\alpha2\beta$ are shown for comparison (taken from Figs 1*D* and 5*A*). *D*, Zn^{2+} concentration–response curves for modulation of half-maximal responses to glycine at GlyR $\alpha1^{T133A}$ and GlyR $\alpha1^{T135A}$ with the wild-type GlyR $\alpha1$ curve for comparison (from Fig. 1*D*). Inset shows glycine currents demonstrating the resistance of GlyR $\alpha1^{T133A}$ to inhibition by 1000 μM Zn^{2+}. $n = 3$–6.

β strand 6 directly below H107 (Fig. 6*A* and *B*). As GlyR $\alpha1$ T133 and T135 residues are ideally located as potential coordinating ligands for Zn^{2+}, they were assessed for their role in Zn^{2+}-mediated inhibition by individual mutation to alanines forming GlyR $\alpha1^{T133A}$ and $\alpha1^{T135A}$. Although GlyR $\alpha1^{T135A}$ exhibited a comparable Zn^{2+} IC_{50} ($29 \pm 2\,\mu$M; $n = 3$) to the wild-type GlyR $\alpha1$ subunit, the GlyR $\alpha1^{T133A}$ mutation ablated Zn^{2+}-mediated inhibition up to 1 mM (Fig. 6*D* and Table 1).

Using the GlyR β subunit to investigate functional asymmetry at the inhibitory Zn^{2+}-binding site

Although a role for the β subunit in coordinating Zn^{2+} has not been favoured previously (Bloomenthal *et al.* 1994; Nevin *et al.* 2003) our data suggested that this subunit subtly influenced the potency of Zn^{2+} at GlyR $\alpha2\beta$

heteromers. Using a different strategy, we assessed the ability of the β subunit to contribute directly to the Zn^{2+}-binding site by examining whether it could, if appropriately mutated at homologous positions, compensate for mutated GlyR $\alpha1$ subunits with reduced Zn^{2+} sensitivities. For example, to compensate for the mutation, GlyR $\alpha1^{H107N}$, with regard to the sidedness of the intersubunit Zn^{2+}-binding site, would require co-expression of the β subunit carrying the mutation, β^{N130H} (Fig. 7, lower schematic diagram). Similarly, the mutant GlyR $\alpha1^{H109F}$ would require pairing with a wild-type β subunit, as this subunit already possesses H132 in the homologous position to H109 in the α subunit (Fig. 7, middle schematic diagram). Finally, the novel GlyR $\alpha1^{T133A}$ mutant could be compensated by the β^{S156T} mutation (Fig. 7, upper schematic diagram). GlyR $\alpha1$ E110 and T112, previously found to influence
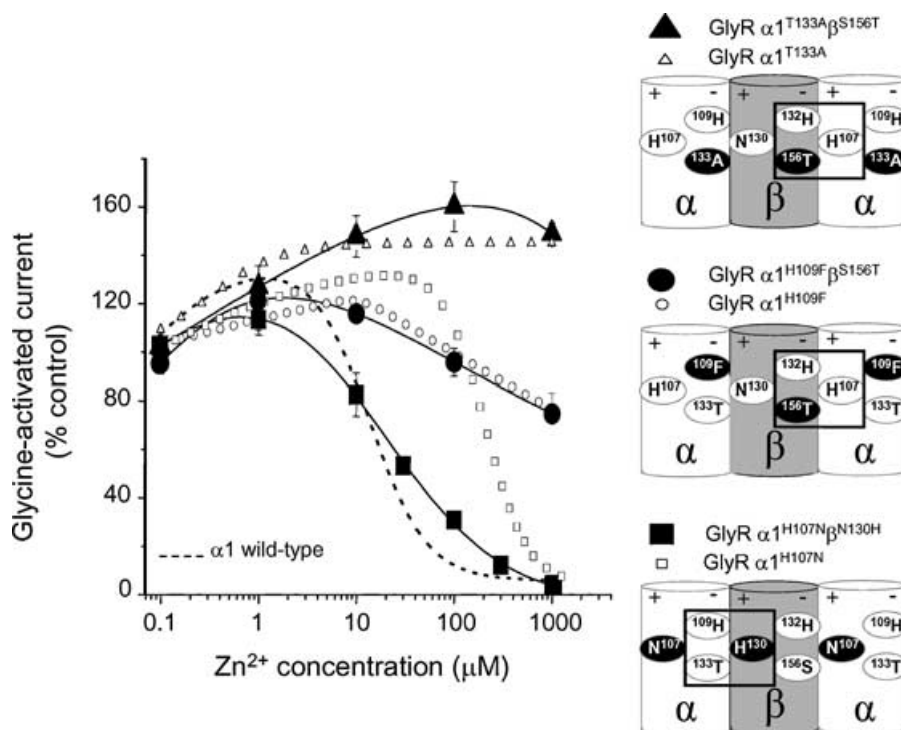

Figure 7. Functional asymmetry at the GlyR α subunit Zn^{2+}-binding site
Zn^{2+} concentration–response curves for the modulation of glycine (EC_{50})-activated currents. Although the co-expressed heteromeric GlyR $\alpha1\beta$ receptors are in each case predicted to have all the necessary components for the Zn^{2+}-binding site reconstituted at the $\alpha\beta$ subunit interface (see schematic diagrams), only when β^{N130H} compensates for $\alpha1^{H107N}$ (lower schematic diagram) is the sensitivity to Zn^{2+}-mediated inhibition recovered. The Zn^{2+} concentration –response curves for GlyR $\alpha1^{H107N}$, $\alpha1^{H109F}$ and $\alpha1^{T133A}$ subunits are included for comparison (data for $\alpha1^{H107N}$ and $\alpha1^{T133A}$ are taken from Figs 2*B* and 5*D*, respectively; $n = 3$–6). The schematic side-view diagrams show part of the GlyR depicting the three examples where a compensatory β subunit (wild-type or mutant) is co-expressed with a GlyR $\alpha1$ subunit lacking one component of the inhibitory Zn^{2+}-binding site (H107, H109 or T133). The mutated residues around the Zn^{2+}-binding site are shown in white on a black background. The corresponding wild-type residues are shown in black on a white background. The rectangles delineate the Zn^{2+}-binding site where all the components under examination have been restored, which occurs at the $\alpha\beta$ subunit interfaces labelled + and – (see text). These schematic diagrams assume that the GlyR is a pentamer where the β subunits are not juxtaposed; however, the predicted $\alpha\beta$ interfaces containing all the components of the inhibitory Zn^{2+} site would still apply even for the unlikely scenario that the two β subunits are juxtaposed.

Zn^{2+}-mediated inhibition (Laube *et al.* 2000), were not investigated in this study as GlyR $\alpha 1^{E110A}$ exerted only a modest 5-fold increase in the Zn^{2+} IC_{50} ($67 \pm 4 \mu M$; $n = 3$) and is predicted to face away from the H107/H109-based Zn^{2+}-binding site (Fig. 6*B*). In addition, T112 (also facing away from the inhibitory site, Fig. 6*B*) has only an indirect effect on Zn^{2+} binding (Nevin *et al.* 2003) and previously, substitutions of this residue have been shown to influence the relative efficacy of partial agonists (Schmieden *et al.* 1999). This suggests that T112 may have a general role in multiple aspects of GlyR function rather than a specific role dedicated to Zn^{2+} coordination.

For the GlyR $\alpha 1$ subunit mutations, H109F and T133A, both of which reside on the same '−' face (using the nomenclature from Fu & Sine, 1996; Fig. 7) of the inhibitory Zn^{2+}-binding site, no recovery of Zn^{2+} potency was observed when either of these subunits were co-expressed with the compensating GlyR β subunits including either H132 or S156T, respectively (IC_{50} values, > 1 mM; $n = 3$; Fig. 7). Furthermore, we investigated this face of the Zn^{2+}-binding site from the perspective of the GlyR $\alpha 1$ T133 residue and found that co-expression of the wild-type GlyR $\alpha 1$ subunit with a β^{S156A} mutant also had no effect on the receptor sensitivity to Zn^{2+}-mediated inhibition (IC_{50}, $17 \pm 7 \mu M$; $n = 3$). These data, accrued from one face (−) of the Zn^{2+}-binding site, concur with the previously reported lack of effect of co-expressing GlyR $\alpha 1$ with β^{H132A} on Zn^{2+}-mediated inhibition (Nevin *et al.* 2003).

In contrast, when the GlyR $\alpha 1^{H107N}$ mutant, which is present on the opposing '+' face of the Zn^{2+}-binding site to H109 and T133, was co-expressed with the GlyR β^{N130H} subunit, a dramatic recovery in Zn^{2+}-mediated inhibition was observed to almost wild-type GlyR $\alpha 1 \beta$ levels of sensitivity (IC_{50}, $24 \pm 3 \mu M$; $n = 5$; Fig. 7). To ensure this mutation was not due to the *de novo* construction of an intrasubunit Zn^{2+}-binding site in the β subunit, as this mutant β^{N130H} subunit alone now contained two juxtaposed histidine residues (H130 and H132), we co-expressed the β^{N130H} subunit with a GlyR $\alpha 1^{H107N,H109F}$ double mutant and this exhibited no recovery to Zn^{2+}-mediated inhibition (IC_{50}, > 1 mM; $n = 4$). This strongly suggested that the β subunit is indeed participating in an intersubunit Zn^{2+}-binding site and that this contribution by the β subunit can only occur from the + face of the subunit.

Discussion

This study has identified a distinct difference in the potency of Zn^{2+}-mediated inhibition between the GlyR $\alpha 1$ and GlyR $\alpha 2$ subunits, which is also seen with the corresponding $\alpha \beta$ subunit heteromers. Comparison of the primary amino acid sequences around the previously deduced inhibitory Zn^{2+}-binding site (Harvey *et al.* 1999)

revealed that a single residue, H107 in the $\alpha 1$ subunit, was likely to be responsible for the different potencies of Zn^{2+}. The absence of this residue in the $\alpha 2$ and $\alpha 3$ subunits substantially accounts for its reduced Zn^{2+} sensitivity, further supporting the assertion that this location on the GlyR is forming a binding site for Zn^{2+}-induced inhibition (Harvey *et al.* 1999; Nevin *et al.* 2003). A previous study comparing Zn^{2+} potency at GlyR $\alpha 1$ and GlyR $\alpha 2$ subunits, in *Xenopus* oocytes, did not report any differences in sensitivity between these subtypes (Laube *et al.* 1995). This could reflect the different expression system, variation in Zn^{2+} application protocols, or possibly the glycine concentrations chosen for modulation by Zn^{2+}, which is acting as a competitive antagonist. However, the data here are supported by the identification of a molecular basis for the differential sensitivity. Moreover, the previously demonstrated increased expression of GlyR $\alpha 1$ over the 'embryonic' $\alpha 2$ during spinal cord development (Hoch *et al.* 1989, 1992), is in accord with the increased sensitivity to Zn^{2+}-mediated inhibition that we observed in older acute spinal cord slices (Becker *et al.* 1988; Takahashi *et al.* 1992; Watanabe & Akagi, 1995). This suggests that the physiological significance of Zn^{2+}-mediated inhibition is unlikely to be relevant at embryonic stages of development as native embryonic GlyRs require more than $50 \mu M$ Zn^{2+} before glycine currents are inhibited. This concurs with a previous report (Laube, 2002) where $50 \mu M$ Zn^{2+} induced only modest inhibition of glycinergic IPSCs in mature spinal cord cultures.

Despite the different sensitivities to inhibitory Zn^{2+}, glycine concentration–response curves for both GlyR $\alpha 1$ and GlyR $\alpha 2$ were displaced in a parallel, competitive-type manner; however, this does not necessarily imply that Zn^{2+} is directly competing for the glycine recognition site, as Zn^{2+} could interact with the receptor in a mutually exclusive allosteric fashion reducing the ability of glycine to bind to its entirely non-overlapping site and vice versa. Indeed, this explanation is consistent with the current views on the discrete locations of the inhibitory Zn^{2+}- and glycine-binding sites (Laube *et al.* 2002). Prior evidence also suggested that Zn^{2+}-mediated inhibition of GlyRs is largely caused by a reduction in the agonist efficacy (E; Laube *et al.* 2000). The values of E reported for glycine at GlyR $\alpha 1$ vary from between 10 and 20 (Laube *et al.* 2000) and 16 (Lewis *et al.* 2003), to 40 (Beato *et al.* 2004) for the higher-liganded GlyR states. By assuming that a sequential ligand-binding site model is sufficient to explain GlyR activation and using this to simulate glycine dose–response curves, a reduction in E alone will not produce parallel displacements in the glycine concentration–response curves of the magnitude observed in our study without significant reductions in the maximum response. For example, for GlyR $\alpha 1$, E would need to be reduced from 40 to 0.19 to increase the glycine

EC_{50} from 24 to 214 μM; however, this would cause the channel open probability (P_o) to be reduced from 0.97 to 0.15, a substantial reduction in the maximum response. Thus it is highly likely that Zn^{2+} is also affecting the affinity of glycine for its recognition site. The Schild analysis here provides the first definitive measurement of Zn^{2+} affinity for the GlyR α1 (pA_2 of 4.44) and indicates that Zn^{2+} has a much lower potency (329-fold) at the glycine receptor compared to the classical competitive GlyR antagonist, strychnine (pA_2, 7.08; K_B, 83.2 nM; Saitoh *et al.* 1994).

Previously, the GlyR β subunit has not been shown to exert any detectable influence on Zn^{2+}-mediated inhibition at GlyR α subunits (Bloomenthal *et al.* 1994; Laube *et al.* 1995; Nevin *et al.* 2003). However, this report demonstrates that in the unique instance of the α2 subtype, co-expression with the β subunit increased the sensitivity to Zn^{2+} inhibition. Although we were unable to attribute this effect to a specific residue in the vicinity of the putative inhibitory Zn^{2+}-binding site, as a consequence we identified GlyR α1 T133 as a vital component for Zn^{2+} inhibition. When considering the location of the intersubunit Zn^{2+}-binding site, in accordance with the three-dimensional GlyR α1 model based on the AChBP, T133 is predicted to reside beneath H109, which is ideal for participating in the putative inhibitory Zn^{2+}-binding site.

Co-expression of GlyR α subunits with complementary β subunits, designed to compensate for α subunits lacking specific components of the inhibitory Zn^{2+}-binding site, revealed an asymmetry of function between the opposing faces of the intersubunit binding site. Effectively 'knocking out' either GlyR α1 H109 or T133, both predicted to be on the same – face of the subunit could not be compensated by β subunits mutated to contain equivalent α subunit residues. This demonstrates that the α subunit H107 + face and the mutant β subunit H132/S156T – face, cannot form a functional Zn^{2+} inhibitory site alone, when the α subunit – face has been disrupted by mutation. In contrast, following knock-out of the GlyR α1 H107 on the opposing + face, the attenuated sensitivity to Zn^{2+}-mediated inhibition was almost fully restored by co-expression with β^{N130H} subunits. The restoration of Zn^{2+}-mediated inhibition for the GlyR α1^{H107N} mutant implies that such inhibition could be mediated from either the GlyR α1 H109/T133 – face or the β N130H + face, or both acting together. As the wild-type GlyR α1 subunit is able to mediate Zn^{2+}-mediated inhibition regardless of the removal of any inhibitory components in the β subunit this means that the H109 and T133 – face of the binding site must be responsible for connecting Zn^{2+} binding to an effect on receptor function (transduction). Furthermore, this transduction must be driven through the GlyR α1 subunit. In comparison, H107 can instead be regarded as a pure binding residue, as this can be donated from a neighbouring subunit that lacks its own Zn^{2+} transduction apparatus i.e. the β subunit.

In the GABA$_A$ receptor the interfacial nature of the high-sensitivity Zn^{2+}-inhibition site along with pharmacological studies has led to the proposal that Zn^{2+} acts to stabilize the closed state of the receptor by stabilizing the interaction between the interfaces (Smart, 1992; Hosie *et al.* 2003). This has also been proposed for the GlyR (Lynch, 2004) and is supported here by the greater potency of inhibitory Zn^{2+} under pre-incubation conditions; that is, Zn^{2+} can access the closed GlyR state and stabilize it before agonist application. Under co-application, glycine activates the receptors before Zn^{2+} can bind, so it must wait until the receptor closes before it can access and stabilize the closed state to induce inhibition. This was manifest in the macroscopic currents by the delayed onset of inhibition. Single-channel studies of the activation mechanism for the GlyR α1 receptor suggest that the higher liganded and open channel state(s) have a higher agonist affinity (Beato *et al.* 2004). Zinc ions might then appear as competitive inhibitors because they stabilize the closed channel state(s) which also has a lower affinity for the agonist. Conversely, agonist activation stabilizes the open channel state(s), where Zn^{2+} cannot induce inhibition by stabilizing the subunit interfaces, so supporting a mutually exclusive, apparently competitive allostery between the agonist and Zn^{2+}-binding sites.

How is this communication transmitted between two quite discrete binding sites? Current structural data for the extracellular domain of the nACh receptor (Unwin *et al.* 2002) suggest that upon agonist activation the inner – faces undergoes significant movement, greater than that at the inner + interface. This conformational flexibility accords with the transduction asymmetry that we have attributed to the Zn^{2+}-binding site, which favours a predominant role for the – face in transducing Zn^{2+} inhibition. From this we would presume that Zn^{2+} stabilizes the GlyR closed state by preventing movement of the – subunit interface relative to the + interface.

With regard to the stoichiometry of glycine and Zn^{2+} binding, the mutually exclusive mechanism suggests that potentially, each site has five copies, one per subunit. However, the number of occupied Zn^{2+} sites required to ensure the receptor remains closed may not necessarily be five. This depends on how the receptor is activated. If a concerted switch of all five subunit extracellular domains is required, then possibly only one Zn^{2+} may be required to stabilize a single subunit interface to prevent this movement. This would seem the most plausible scenario because the GlyRα1β heteromers retain the same sensitivity and efficacy for Zn^{2+}-mediated inhibition as the α1 homomer, even though the β sub-unit lacks homologous Zn^{2+}-binding residues within the inhibitory site. Thus two to three Zn^{2+}-binding sites

contributed by the α subunits appear to be sufficient, in agreement with a previous study using mixed homomeric $\alpha 1$ receptors with disrupted Zn^{2+}-binding sites (Nevin *et al.* 2003).

Taken overall, this study identifies Zn^{2+} as a useful pharmacological tool to distinguish between GlyR $\alpha 1$ and $\alpha 2$ or $\alpha 3$ subunits. It also provides a rationale by which Zn^{2+} binding initiates the transduction of Zn^{2+}-mediated inhibition resulting in an effect on glycine binding to the receptor. This appears to be propagated asymmetrically from the Zn^{2+}-binding site being driven from the – face. This phenomenon of asymmetric propagation of signal transduction is quite likely to be a common feature characterizing the binding of ligands to many different sites on ligand-gated ion channels.

References

Aprison MH & Daly EC (1978). Biochemical aspects of transmission at inhibitory synapses: the role of glycine. In *Advances in Neurochemistry*, Vol. 3, pp. 203–294, ed. Agranoff BW & Aprisan MH. Plenum Press, New York.

Arunlakshana O & Schild HO (1959). Some quantitative uses of drug antagonists. *Br J Pharmacol* **14**, 48–58.

Assaf SY & Chung SH (1984). Release of endogenous Zn^{2+} from brain tissue during activity. *Nature* **308**, 734–736.

Auld DS (2001). Zinc coordination sphere in biochemical zinc sites. *Biometals* **14**, 271–313.

Beato M, Groot-Kormelink PJ, Colquhoun D & Sivilotti LG (2004). The activation mechanism of alpha1 homomeric glycine receptors. *J Neurosci* **24**, 895–906.

Becker CM, Hoch W & Betz H (1988). Glycine receptor heterogeneity in rat spinal cord during postnatal development. *EMBO J* **7**, 3717–3726.

Bloomenthal AB, Goldwater E, Pritchett DB & Harrison NL (1994). Biphasic modulation of the strychnine-sensitive glycine receptor by Zn^{2+}. *Mol Pharmacol* **46**, 1156–1159.

Brejc K, van Dijk WJ, Klaassen RV, Schuurmans M, van Der OJ, Smit AB & Sixma TK (2001). Crystal structure of an ACh-binding protein reveals the ligand-binding domain of nicotinic receptors. *Nature* **411**, 269–276.

Celentano JJ, Gibbs TT & Farb DH (1988). Ethanol potentiates GABA- and glycine-induced chloride currents in chick spinal cord neurons. *Brain Res* **455**, 377–380.

Draguhn A, Verdoorn TA, Ewert M, Seeburg PH & Sakmann B (1990). Functional and molecular distinction between recombinant rat GABA$_A$ receptor subtypes by Zn^{2+}. *Neuron* **5**, 781–788.

Frederickson CJ, Suh SW, Silva D, Frederickson CJ & Thompson RB (2000). Importance of zinc in the central nervous system: the zinc-containing neuron. *J Nutr* **130**, 1471S–1483S.

Fu DX & Sine SM (1996). Asymmetric contribution of the conserved disulphide loop to subunit oligomerisation and assembly of the nicotinic acetylcholine receptor. *J Biol Chem* **271**, 31479–31484.

Grenningloh G, Gundelfinger E, Schmidt B, Betz H, Dorlison MG & Barnard EA, Schofield PR & Seeburg PH (1987). Glucine vs GABA receptors. *Nature* **330**, 25–26.

Han Y & Wu SM (1999). Modulation of glycine receptors in retinal ganglion cells by zinc. *Proc Natl Acad Sci U S A* **96**, 3234–3238.

Handford CA, Lynch JW, Baker E, Webb GC, Ford JH, Sutherland GR & Schofield PR (1996). The human glycine receptor β subunit: primary structure, functional characterisation and chromosomal localisation of the human and murine genes. *Brain Res Mol Brain Res* **35**, 211–219.

Harrison NL & Gibbons SJ (1994). Zn^{2+}: an endogenous modulator of ligand- and voltage-gated ion channels. *Neuropharmacology* **33**, 935–952.

Harrison NL, Kugler JL, Jones MV, Greenblatt EP & Pritchett DB (1993). Positive modulation of human ?-aminobutyric acid type A and glycine receptors by the inhalation anesthetic isoflurane. *Mol Pharmacol* **44**, 628–632.

Harvey RJ, Thomas P, James CH, Wilderspin A & Smart TG (1999). Identification of an inhibitory Zn^{2+} binding site on the human glycine receptor alpha1 subunit. *J Physiol* **520**, 53–64.

Hoch W, Betz H & Becker CM (1989). Primary cultures of mouse spinal cord express the neonatal isoform of the inhibitory glycine receptor. *Neuron* **3**, 339–348.

Hoch W, Betz H, Schramm M, Wolters I & Becker CM (1992). Modulation by NMDA receptor antagonists of glycine receptor isoform expression in cultured spinal cord neurons. *Eur J Neurosci* **4**, 389–395.

Hosie AM, Dunne EL, Harvey RJ & Smart TG (2003). Zinc-mediated inhibition of GABA$_A$ receptors: discrete binding sites underlie subtype specificity. *Nat Neurosci* **6**, 362–369.

Howell GA, Welch MG & Frederickson CJ (1984). Stimulation-induced uptake and release of zinc in hippocampal slices. *Nature* **308**, 736–738.

Kay AR (2003). Evidence for chelatable zinc in the extracellular space of the hippocampus, but little evidence for synaptic release of Zn^{2+}. *J Neurosci* **23**, 6847–6855.

Laube B (2002). Potentiation of inhibitory glycinergic neurotransmission by Zn^{2+}: a synergistic interplay between presynaptic P2X$_2$ and postsynaptic glycine receptors. *Eur J Neurosci* **16**, 1025–1036.

Laube B, Kuhse J & Betz H (2000). Kinetic and mutational analysis of Zn^{2+} modulation of recombinant human inhibitory glycine receptors. *J Physiol* **522**, 215–230.

Laube B, Kuhse J, Rundstrom N, Kirsch J, Schmieden V & Betz H (1995). Modulation by zinc ions of native rat and recombinant human inhibitory glycine receptors. *J Physiol* **483**, 613–619.

Laube B, Maksay G, Schemm R & Betz H (2002). Modulation of glycine receptor function: a novel approach for therapeutic intervention at inhibitory synapses? *Trends Pharmacol Sci* **23**, 519–527.

Lewis TM, Schofield RP & McClellan AM (2003). Kinetic determinants of agonist action at the recombinant human glycine receptor. *J Physiol* **549**, 361–374.

Lynch JW (2004). Molecular structure and function of the glycine receptor chloride channel. *Physiol Rev* **84**, 1051–1095.

Mangin JM, Baloul M, Prado DC, Rogister B, Rigo JM & Legendre P (2003). Kinetic properties of the $\alpha2$ homo-oligomeric glycine receptor impairs a proper synaptic functioning. *J Physiol* **553**, 369–386.

Miller PS, Harvey RJ & Smart TG (2004). Differential agonist sensitivity of glycine receptor $\alpha2$ subunit splice variants. *Br J Pharmacol* **143**, 19–26.

Nevin ST, Cromer BA, Haddrill JL, Morton CJ, Parker MW & Lynch JW (2003). Insights into the structural basis for zinc inhibition of the glycine receptor. *J Biol Chem* **278**, 28985–28992.

Pfeiffer F, Graham D & Betz H (1982). Purification by affinity chromatography of the glycine receptor of rat spinal cord. *J Biol Chem* **257**, 9389–9393.

Pribilla I, Takagi T, Langosch D, Bormann J & Betz H (1992). The atypical M2 segment of the α subunit confers picrotoxinin resistance to inhibitory glycine receptor channels. *EMBO J* **11**, 4305–4311.

Saitoh T, Ishida M, Maruyama M & Shinozaki H (1994). A novel antagonist, phenylbenzene omega-phosphono-alpha-amino acid, for strychnine-sensitive glycine receptors in the rat spinal cord. *Br J Pharmacol* **113**, 165–170.

Schmieden V, Grenningloh G, Schofield PR & Betz H (1989). Functional expression in Xenopus oocytes of the strychnine binding 48 kd subunit of the glycine receptor. *EMBO J* **8**, 695–700.

Schmieden V, Kuhse J & Betz H (1999). A novel domain of the inhibitory glycine receptor determining antagonist efficacies: further evidence for partial agonism resulting from self-inhibition. *Mol Pharmacol* **56**, 464–472.

Smart TG (1992). A novel modulatory binding site for zinc on the GABA$_A$ receptor complex in cultured rat neurones. *J Physiol* **447**, 587–625.

Smart TG, Hosie AM & Miller PS (2004). Zn^{2+} ions: modulators of excitatory and inhibitory synaptic activity. *Neuroscientist* **10**, 432–442.

Smart TG, Moss SJ, Xie X & Huganir RL (1991). GABA$_A$ receptors are differentially sensitive to zinc: dependence on subunit composition. *Br J Pharmacol* **103**, 1837–1839.

Smart TG, Xie X & Krishek BJ (1994). Modulation of inhibitory and excitatory amino acid receptor ion channels by zinc. *Prog Neurobiol* **42**, 393–341.

Takahashi T, Momiyama A, Hirai K, Hishinuma F & Akagi H (1992). Functional correlation of fetal and adult forms of glycine receptors with developmental changes in inhibitory synaptic receptor channels. *Neuron* **9**, 1155–1161.

Unwin N, Miyazawa A, Li J & Fujiyoshi Y (2002). Activation of the nicotinic acetylcholine receptor involves a switch in conformation of the alpha subunits. *J Mol Biol* **319**, 1165–1176.

Watanabe E & Akagi H (1995). Distribution patterns of mRNAs encoding glycine receptor channels in the developing rat spinal cord. *Neurosci Res* **23**, 377–382.

Acknowledgements